Available online at www.sciencedirect.com
ScienceDirect
Journal of the European Ceramic Society 29 (2009) 1809–1815
www.elsevier.com/locate/jeurceramsoc

Oxidation behaviour of a pressureless sintered HfB_2–$MoSi_2$ composite

Diletta Sciti *, Andrea Balbo, Alida Bellosi

CNR-ISTEC, Institute of Science and Technology for Ceramics, Via Granarolo 64, I-48018 Faenza, Italy

Received 28 July 2008; received in revised form 22 September 2008; accepted 24 September 2008
Available online 5 November 2008

Abstract

The thermal stability of a 80-vol.% HfB_2 + 20 vol.% $MoSi_2$ composite is tested under oxidizing environment. Oxidation tests are carried out in flowing synthetic air in a TG equipment from 1000 to 1400 °C with exposure time of 30 h. At temperatures ≥1200 °C the silica resulting from oxidation of molybdenum disilicide seals the sample surface, preventing hafnium diboride from fast degradation. Analysis of the kinetics is carried out through fitting of the thermogravimetric curves. Between 1200 and 1400 °C, the kinetic curves deviate from a parabolic behaviour, being more close to a logarithmic–parabolic behaviour.

Keywords: Ceramic; Microstructure; Oxidation; Borides

1. Introduction

Hafnium diboride is gaining increasing attention as a highly refractory compound with superior properties at high temperature. Nowadays the design and production of new materials suitable to withstand high temperatures are stimulated by an increasing demand for applications in the field of thermal protection systems and for several industrial sectors like foundry. HfB_2-based composites display a number of unique properties including hardness, high thermal and electrical conductivity and chemical stability.[1–12] HfB_2–SiC composites are able to withstand very high temperatures[5–7] and can maintain their room temperature strength up to 1500 °C in air.[6,7] The addition of $MoSi_2$ to borides seems to be very promising as it allows the densification of composites by pressureless sintering and the resulting composites retain their strength up to 1500 °C.[10,11] HfB_2–$MoSi_2$ composites have also been tested in an arc jet facility at 1900 °C showing excellent stability due to the development of a silica-based scale.[12] So far, oxidation studies reported in the literature have concerned pure HfB_2,[13,14] HfB_2–SiC[5,8] materials, and HfB_2–Si_3N_4[15] materials. Oxidation data for pure HfB_2 between 1200 and 1700 °C could be fitted to a parabolic rate equation. Around 1700 °C there was an abrupt increase of the oxidation rate due to transition from monoclinic to tetragonal HfO_2.[13] More recently, a mechanistic model that interprets the oxidation behaviour of Zr and Hf borides in the range 1000–1800 °C has been formulated.[14] At temperature below 1400 °C, the rate limiting step is the diffusion of dissolved oxygen through liquid boria, while at higher temperatures boria is lost by evaporation and the oxidation rate is limited by diffusion of molecular oxygen between columnar blocks of HfO_2.[14] Silica has very low diffusivities for oxygen and is a very protective scale at moderate temperatures. Hence, SiC, Si_3N_4 and transition metal silicides are considered very useful additives for improving the oxidation resistance in the middle temperature range. HfB_2–SiC materials[5,8] were reported to withstand temperatures as high as 1700 °C thanks to the formation of a borosilicate glass containing HfO_2 crystals, which is an effective barrier against the inward diffusion of oxygen. For HfB_2–Si_3N_4 materials oxidation studies were carried out[15] up to 1400 °C. At temperatures in the 900–1200 °C range, the main oxidation products were HfO_2, B_2O_3 and borosilicate glass. In the 1200–1400 °C range, SiO_2 and $HfSiO_4$ were detected. Kinetic curves recorded at 1450 and 1600 °C were shown to be parabolic.In this work, the oxidation behaviour of a HfB_2-20 vol.% $MoSi_2$ composite is tested in the middle temperature range, i.e. between 1000 and 1400 °C. Actually, $MoSi_2$ was already found to be beneficial for improving the oxidation resistance of ZrB_2–20 vol.% $MoSi_2$ composites in the same temperature range.[16–18]

* Corresponding author. Tel.: +39 0546699748 fax: +39 054646381.
E-mail address: diletta.sciti@istec.cnr.it (D. Sciti).

0955-2219/$ – see front matter © 2008 Elsevier Ltd. All rights reserved.
doi:10.1016/j.jeurceramsoc.2008.09.018

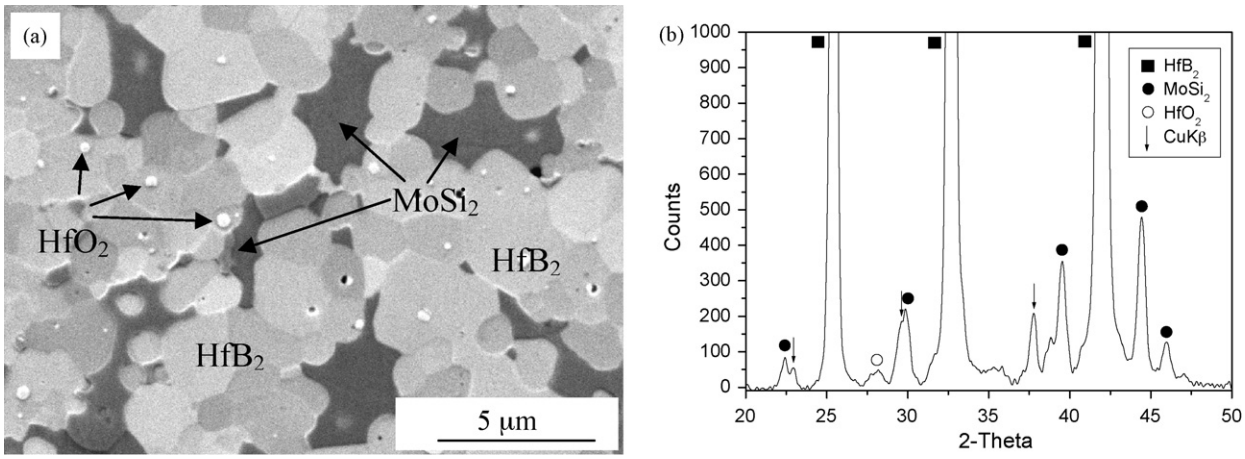

Fig. 1. (a) Polished microstructure and (b) X-ray diffraction of as-sintered HfB_2–20 vol.% $MoSi_2$.

2. Experimental procedure

2.1. Material

Commercial powders were used for the preparation of the composite material: HfB_2 (Cerac Incorporated, Milwaukee, USA), particle size range 0.5–5 μm. Impurities: Al (0.07%), Fe (0.01%), Zr (0.47%); $MoSi_2$ (<2 μm, Aldrich, Milwaukee, USA), mean particle size 2.8 μm and oxygen content of about 1 wt.%. Dense pellets were prepared by pressureless sintering at 1950 °C. Details on the material's processing are reported elsewhere.[11]

2.2. Oxidation tests

Rectangular plates sized 9.0 mm × 8.0 mm × 1.0 mm were cut from the sintered pellet. The specimens were cleaned in ultrasonicated acetone bath, dried and weighed (accuracy 0.01 mg). The oxidation tests were carried out in a thermogravimetric analyser (model STA449, NETSCH, Geraetebau GmbH, Selb, Germany), in synthetic air (composition: 80 vol.% N_2 + 20 vol.% O_2, with 30 ml/min gas flow) between 1000 to 1400 °C with isothermal exposure time of 30 h for each experiment, heating rate 30 °C/min and free cooling. The fast heating-up stage prior to the isothermal period was applied to minimize oxidation effects before reaching the target temperatures. The mass variation was recorded continuously with 10^{-3} mg of sensitivity. The TG measurements evaluation was performed with the subtraction of Buoyancy effect corrections. As-sintered and oxidized sample surfaces were analysed by X-ray diffraction (Cu Kα radiation, Miniflex Rigaku, Tokyo, Japan). Surfaces and polished cross-sections were analysed by scanning electron microscope (SEM, Leica Cambridge S360, Cambridge, UK) and energy dispersive microanalysis (EDS, Model INCA energy 300; Oxford Instruments, High Wycombe, UK).

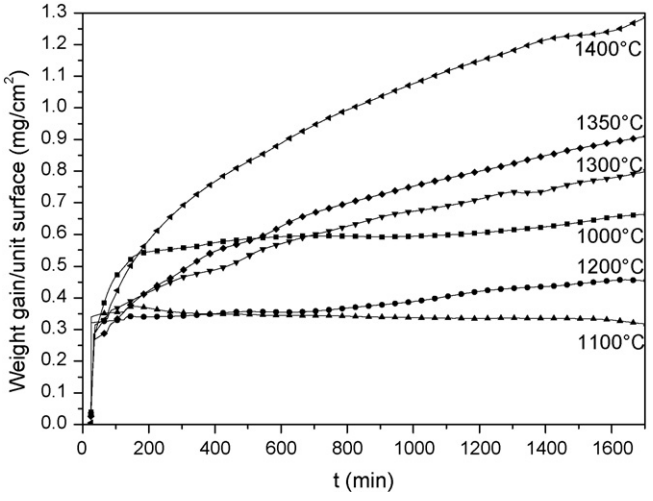

Fig. 2. Thermogravimetric curves of the HfB_2–20 vol.% $MoSi_2$ composite in the range 1000–1400 °C.

3. Results

3.1. Microstructure of the as-sintered material

The sintered material contained a low amount of residual porosity, 2%, as ascertained by SEM analysis and density measurements. Crystalline HfB_2, $MoSi_2$ and traces of HfO_2 were identified by X-ray diffraction (Fig. 1a). An example of the polished section is displayed in Fig. 1b. HfB_2 grains have a rounded shape while the $MoSi_2$ phase has a very irregular morphology with very low dihedral angles. This peculiar characteristic indicates that $MoSi_2$ was very ductile at the sintering temperature or could have formed a liquid phase, which is not surprising since the sintering temperature was close to its melting point (2020 °C). The analysis of secondary phases by EDS confirmed the presence of HfO_2, HfC and traces of a Mo–B phase. Further details are reported elsewhere.[11]

3.2. Oxidation curves

Thermogravimetric curves recorded during the oxidation of the composite 80 vol.% HfB_2 + 20 vol.% $MoSi_2$ are displayed in Fig. 2. With the exception of the curve collected at 1100 °C showing a mass loss, in all of the cases a weight gain was recorded. The weight gain after oxidation at 1200 °C was

lower than after oxidation at 1000 °C. It was found that none of the recorded kinetics followed a simple law, i.e. linear or parabolic. Hence, kinetic curves were fitted according to a multiple law model including a linear, parabolic and logarithmic contribution[18]:

$$\frac{\Delta W}{S} = K_{\text{par}} \cdot t^{1/2} + K_{\text{lin}} \cdot t + K_{\log} \cdot \log(t) \quad (1)$$

where $\Delta W/S$ is the weight gain per unit surface, K_{par}, K_{lin}, $K_{\log}$ are the parabolic, linear and logarithmic term, respectively. The physical meaning of Eq. (1) is that different phenomena can simultaneously take place during oxidation, such as diffusion of inward and outward species, rupture of the scale, crystallization of new phases inside the scale, evaporation of scale material, etc.[18] Ceramic composites are highly unlikely to show a simple oxidation behaviour, thus a multiple regression analysis seems to be more suitable for the interpretation of experimental data. With the exception of the linear term (K_{lin}) which can be negative when significant development of gaseous products occurs, negative K parameters do not reflect a physical reality.

The experimental data and the fitting curves are displayed in Fig. 3a–f. Kinetic parameters and fit goodness values, R^2, are reported in Table 1. The oxidation kinetics recorded at temperatures of 1000 and 1100 °C cannot be properly fitted by Eq. (1) either because the R^2 values (fit goodness) are too low or because K parameters assume negative values. The most

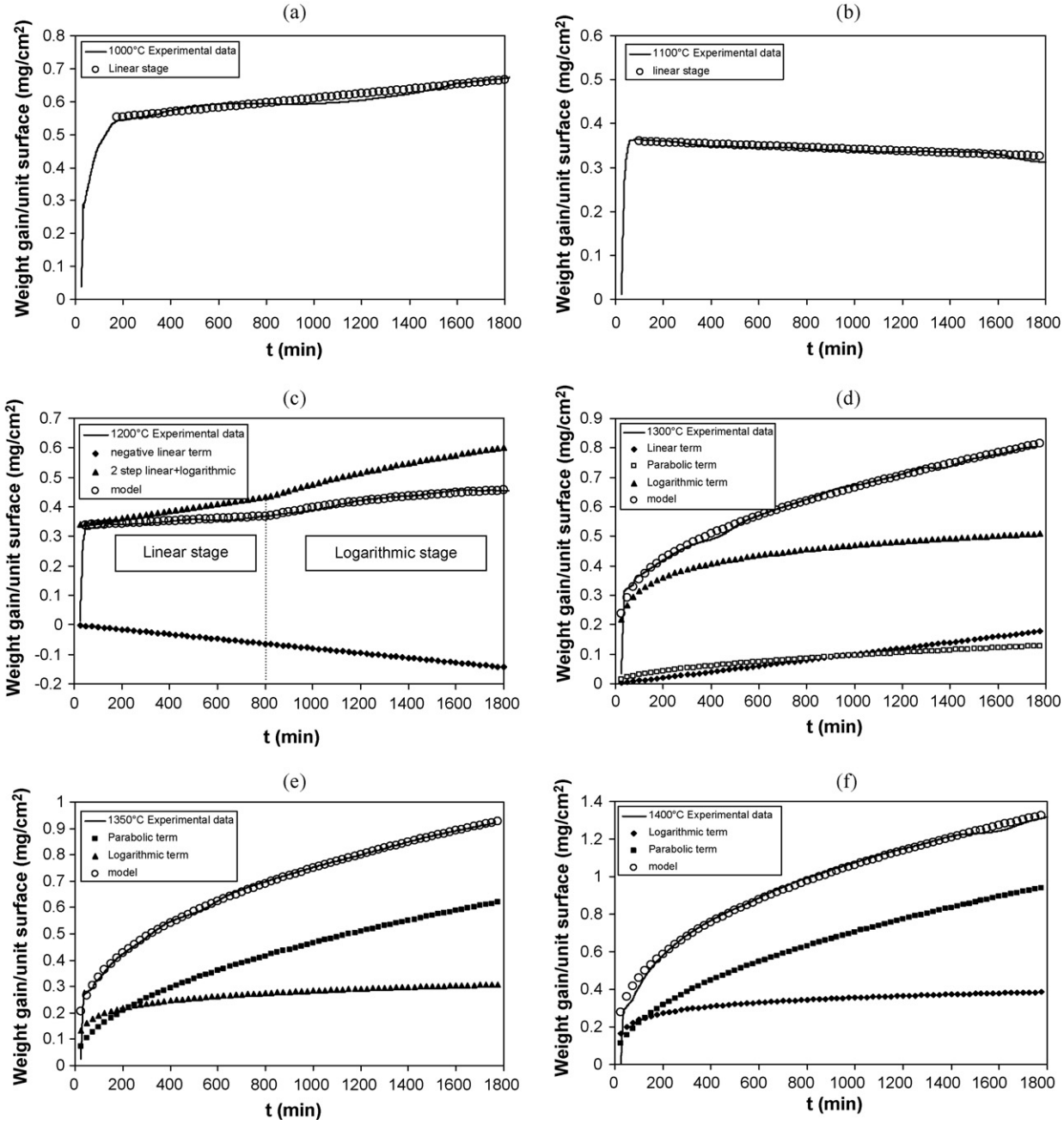

Fig. 3. (a–f) Fitting of the thermogravimetric curves in the range 1000–1400 °C. The model is the sum of the linear, parabolic, logarithmic contributions.

Table 1
Kinetic parameters of the oxidation fitting curve, relatively to linear (K_{lin}), parabolic (K_{par}) and logarithmic (K_{log}) contributions and R^2 (fit goodness) values.

Oxidation temperature (°C)	K_{lin} (mg cm^{-2} min^{-1})	K_{par} (mg cm^{-2} min$^{-1/2}$)	K_{log}	R^2
1000	6.6×10^{-5}	–	–	0.905
1100	-2×10^{-5}			0.960
1200 ($0 < t < 800$)	-8×10^{-5}	–	–	0.975
1200 ($t > 800$ min)	-8×10^{-5}	–	0.49	0.994
1300	1×10^{-4}	0.003	0.16	0.988
1350	–	0.015	0.09	0.997
1400	–	0.022	0.12	0.992

reasonable solution is a linear behaviour starting after a transition stage, as shown in Fig. 3a and b. During oxidation at 1000 °C a weight gain is observed, while at 1100 °C the negative linear term indicates that an overall mass loss occurs, i.e. reactions leading to mass loss prevail on reactions leading to mass gain. The interpretation of the kinetic curve at 1200 °C is quite difficult. The fit with Eq. (1) produces a negative logarithmic term which is not physically acceptable. The data seem to indicate that two subsequent stages occur during oxidation. The fit with Eq. (1) however does not allow for a shift in time after which a new law acts exclusively, but interprets the data in terms of different kinetics acting at the same time. Thus, in Fig. 3c the experimental data are interpreted in terms of a linear stage occurring for $100 < t < 800$ min and a logarithmic stage occurring for $t > 800$ min. The curve recorded at 1300 °C was successfully fitted by Eq. (1), as displayed in Fig. 3d. The plot shows the separate contributions of the linear, parabolic and logarithmic term and their sum, which is overlapped to the experimental data. As can be seen, the 1300 °C kinetics is dominated by the logarithmic term. At 1350 and 1400 °C, the data can be fitted by Eq. (1), but the linear term assumes negative values. Assuming that at these temperatures no significant loss of gaseous species occurs due to formation of a stable oxide, a logarithmic–parabolic curve is the best fitting solution for the experimental data (Fig. 3e and f).

3.3. Oxidation product

The crystalline phases formed after oxidation are shown in Fig. 4. The morphological evolution of surfaces and cross-sections is reported in Figs. 5a–d and 6a–d.

For samples oxidized in the temperature range 1000–1200 °C, monoclinic HfO_2 was the main crystalline product due to oxidation. In the 1300–1400 °C oxidation range, beside HfB_2 from the bulk, HfO_2 and $HfSiO_4$ were detected. A slight reduction of HfB_2 peaks intensity was observed upon oxidation at 1400 °C, due to thickening of the surface scale, as illustrated later.

In the investigated temperature range, all the sample surfaces were covered by a continuous borosilicatic glassy layer, in which small crystals (HfO_2/$HfSiO_4$) were dispersed (Fig. 5). This layer had a thickness of less than a few micrometers and completely sealed the sample surface. The presence of boron was clearly detected by EDS after oxidation at 1300–1400 °C, (see inset in Fig. 5c). Increasing wrinkling of the surface oxide was observed with increasing the oxidation temperature, due to formation of gaseous products.

The polished cross-sections (Fig. 6) give further indications. Upon oxidation at 1000 °C, a 1-μm thick silica-based layer forms. The coverage is irregular and hafnium oxide crystals are observed. Upon oxidation at 1100 and 1200 °C, the surface scale has a thickness of about 2–4 μm. In the 1300–1400 °C range, formation of bubbles on the surface becomes more evident and, despite the presence of the surface oxide, subsurface oxidation takes place. The surface borosilicate glass has a very irregular thickness of about 5–10 μm, irrespective of the oxidation temperature. The subsurface modified layer has a thickness which increases from 10 to 20 μm increasing the oxidation temperature from 1300 to 1400 °C. In this intermediate layer penetration of the glassy phase and formation of molybdenum oxide (MoO) or MoB or a mixed MoOB phase is observed, as shown in Fig. 6. The morphology of these phases suggests solidification from a liquid phase.

4. Discussion

In this paragraph a correlation between TG curves, XRD data and SEM analyses is attempted. The oxidation reactions occur-

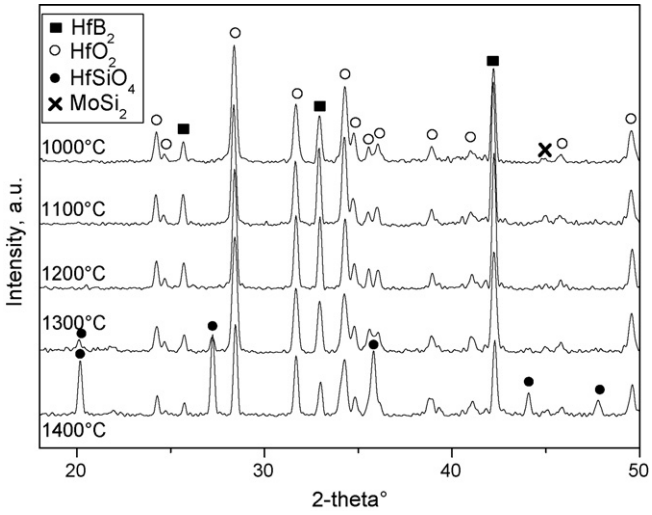

Fig. 4. X-ray diffraction of the sample after oxidation in the range 1000–1400 °C.

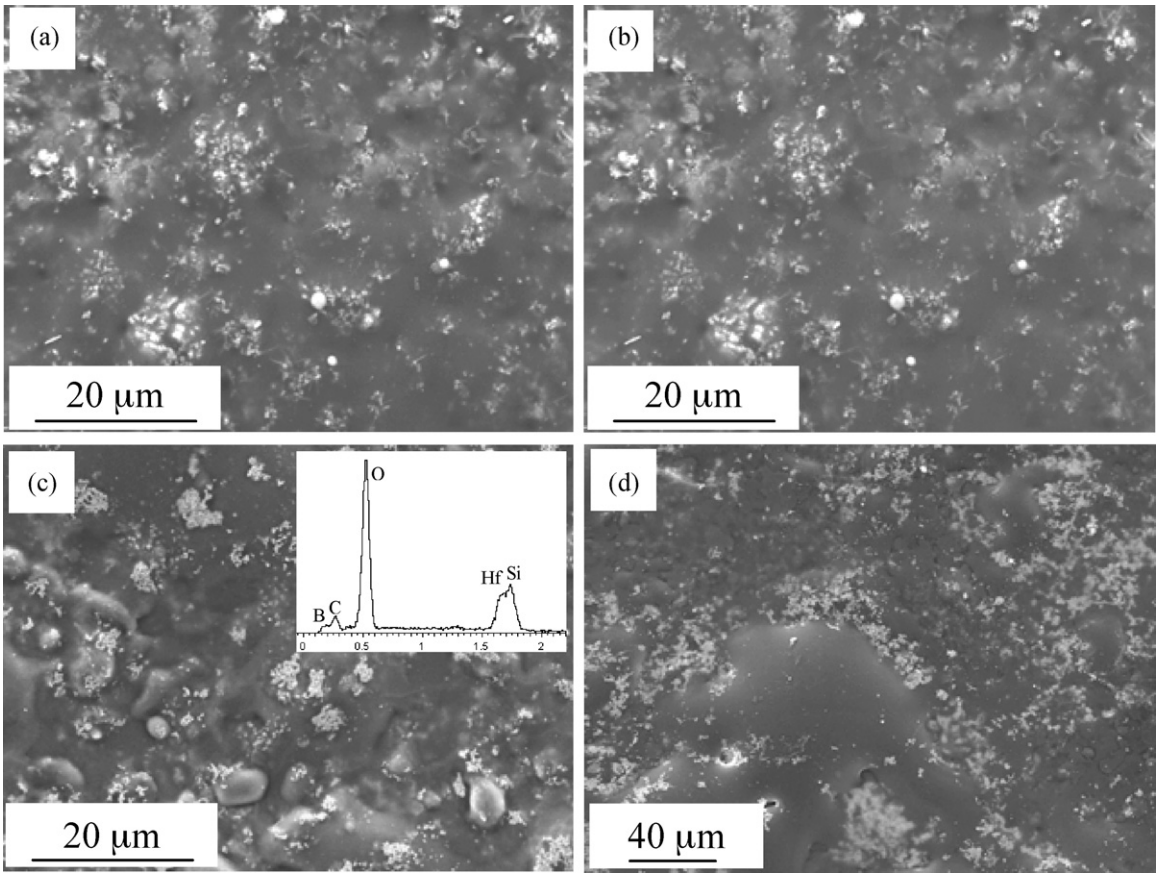

Fig. 5. SEM analysis of oxidized surfaces at: (a) 1100 °C, (b) 1200 °C, (c) 1300 °C and (d) 1400 °C. Inset: EDS spectrum of the surface.

ring in the HfB_2–$MoSi_2$ composite during high-temperature treatments in air depend on the oxidation reactions of the two constituent phases and on further interactions among their oxide products. HfB_2 oxidizes according to the following reactions[13]:

$$HfB_2(s) + (5/2)O_2\ (g) = HfO_2\ (s) + B_2O_3\ (l), \quad (1)$$

$$B_2O_3\ (l) = B_2O_3\ (g). \quad (2)$$

At temperature >1100 °C, liquid boria starts to vaporize.[13] The oxidized surface is constituted of a hafnia-based layer. $MoSi_2$ has an excellent oxidation resistance at temperatures >1000 °C because of a protective silica surface layer[17]:

$$MoSi_2\ (s) + (7/2)\ O_2\ (g) = 2SiO_2\ (s) + MoO_3\ (s). \quad (3)$$

In the subsurface layer, at $T \geq 1300$ °C, liquid boria from reaction (1) can further react with $MoSi_2$, to form MoB or MoOB or MoO species, in agreement with SEM observations.

In the composite of the present work, according to microstructural observations, the oxidation during isothermal runs in the tested temperature range can be explained as follows.

- 1000 °C: The oxidation of HfB_2 into HfO_2 according to reactions (1 and 2) and formation of silica from reaction (3) are the dominant effects. Liquid B_2O_3 is known to have a protective effect, while HfO_2 is semi-protective due to its anion deficiency.[13] Due to the low thickness of the oxidized layer, loss of volatile species cannot be ruled out. The roughly linear behaviour suggests that the scale is not fully protective.
- 1100 °C: The negative linear kinetic curve indicates that loss of volatile species prevails. The evaporation of liquid boria is thought to play a major role at this temperature (reaction (2)). The morphology of the oxidized layer and X-ray diffraction data indicate the formation of a glassy layer embedding hafnia crystals. The glassy layer, however, is probably too thin to exert an efficient protective action.
- 1200 °C: As previously observed, the weight gain at the end of the isothermal stage is lower than at 1000 and 1100 °C. At this temperature, evaporation of liquid boria should be the dominant mechanism but SEM analyses demonstrate the formation of a continuous surface glassy layer. During the first stage controlled by linear kinetics (for 100 min $< t <$ 800 min) the formed scale could be too thin to effectively protect the sample from mass loss due to evaporation of liquid boria, hence weight gain and weight loss phenomena occur simultaneously. During the second stage ($t >$ 800 min), the formation of a stable silica-based scale starts to limit gas evolution and hence the kinetics has a decelerating feature, being the superimposition of a negative linear term and a positive logarithmic term.
- 1300–1400 °C: In this temperature range, the major contribution to the weight gain comes from the formation of a

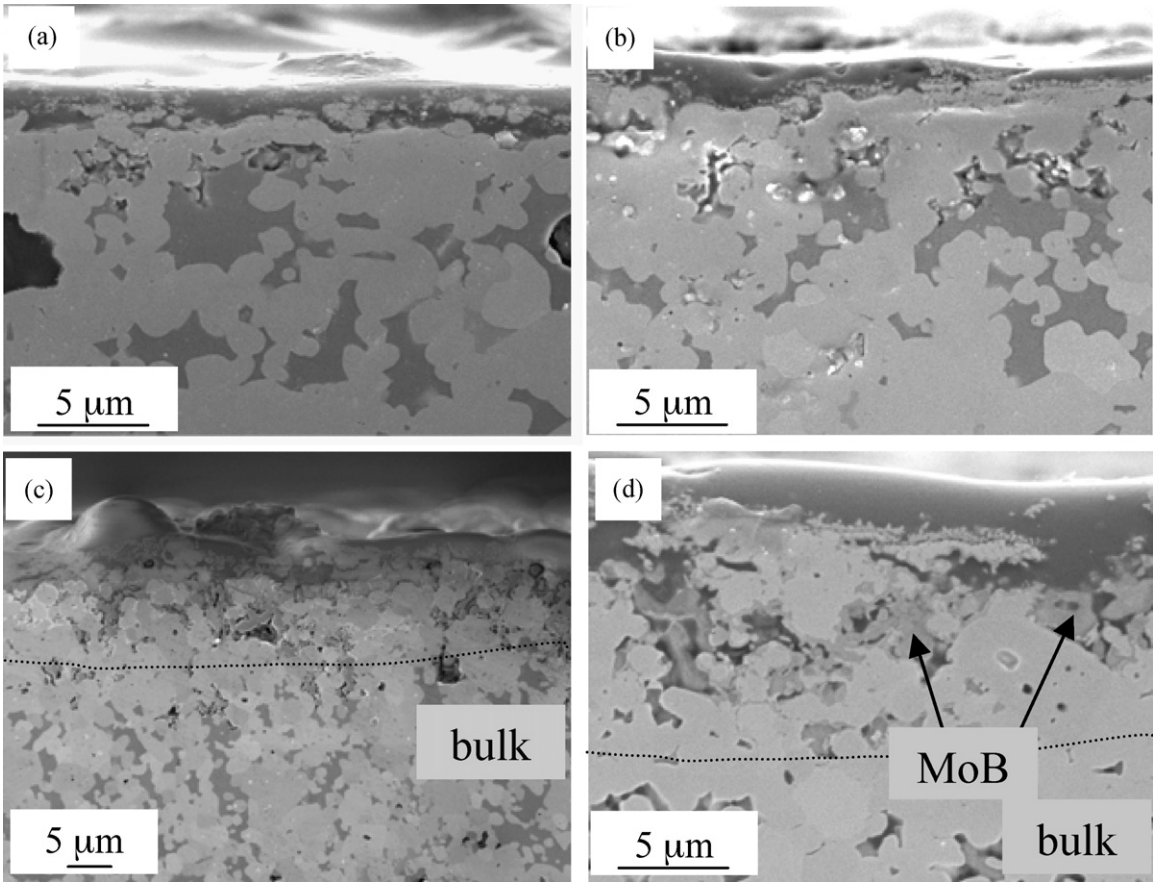

Fig. 6. SEM analysis of oxidized sections at: (a) 1100 °C, (b) 1200 °C, (c) 1300 °C and (d) 1400 °C.

SiO_2-rich glass that increases in thickness with increase of the oxidation temperature. Furthermore, we have observed the formation of hafnon crystals. Since HfO_2 crystals are embedded in a continuous and partially amorphous silica-rich layer, further reaction can occur among the oxidation products to form crystalline $HfSiO_4$. Similar to the mechanism of formation of zircon,[20] when HfO_2 grains are embedded in a silica layer, interstitial silicon diffuses and dissolves into crystalline hafnia until the solubility limit is reached, thereafter $HfSiO_4$ crystals precipitate. The decelerated kinetics at 1300 °C contains a strong logarithmic term. Logarithmic oxidation is thought to set in when the oxide begins to crystallize because the decrease of the amorphous phase leads to a decrease of the effective oxidation cross-section, thus reducing the oxidation rate constant.[19,21] In the composite analysed, the logarithmic term could account for the crystallization of hafnon from HfO_2 and glassy silica. The kinetics recorded at 1350 and 1400 °C are still far from a parabolic behaviour, but it can be observed that the logarithmic component tends to decrease and the parabolic component to increase. The parabolic term can be explained in terms of diffusion of oxygen through the glassy layer.[18] The logarithmic contribution derives from the crystallization of hafnon in the glassy scale.

Oxidation data collected for the HfB_2–20 vol.% $MoSi_2$ composite, can be compared with data from a ZrB_2–20 vol.% $MoSi_2$ composite, which was tested in oxidizing environment using the same experimental conditions of the present work.[20] Compared to the ZrB_2-based system, the weight gain after 30 h of isothermal run is notably reduced. At 1200 °C it is about 1/2 of the ZrB_2 weight gain, at 1300 °C 1/4, at 1400 °C 1/5. A direct comparison of the weight gain after isothermal stage at 1400 °C is

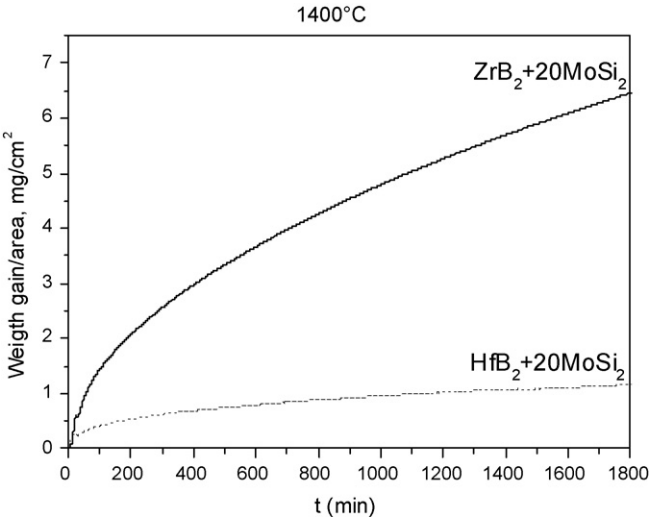

Fig. 7. Comparison of weight gain behaviour between ZrB_2–$MoSi_2$ and HfB_2–$MoSi_2$ composites.

shown in Fig. 7. Since the secondary phase type and amount is the same for the two composites, it must be concluded that the higher stability of the HfB_2-composite is related to the oxidation resistance of the matrix. This feature was already found in the study of monolithic ZrB_2 and HfB_2.[13] Besides, for both systems, the weight gain at 1200 °C is lower than at 1000 °C due to formation of the protective silica scale. Other similarities concern the formation of MoB in the subsurface layer and the formation of zircon (hafnon) in the silica scale at 1300–1400 °C. However, differently from the logarithmic curves displayed by the HfB_2–$MoSi_2$ system, the kinetics of the ZrB_2–$MoSi_2$ system are mostly parabolic in the 1200–1400 °C temperature range, indicating that the dominant mechanism is diffusion of oxygen through the silica-based oxide layer and that other phenomena such as crystallization of the scale play a minor role.

5. Conclusions

Oxidation tests carried out in a thermogravimetric analyser proved that the composite 80 vol.% HfB_2 + 20 vol.% $MoSi_2$ can withstand temperatures up to 1400 °C under oxygen-containing environment. At lower temperatures (1000–1200 °C), Hafnium oxide is the main oxidation product. At temperatures ≥1200 °C, owing to the oxidation of $MoSi_2$, appreciable amounts of glass form, which improves the oxidation resistance of the material. The kinetic curves generally deviate from a parabolic behaviour, being more close to a logarithmic–parabolic behaviour, which is the result of the complex reactions occurring in the scale. Compared to the previously analysed ZrB_2-20 vol.% $MoSi_2$, the HfB_2-based composite shows a higher stability.

Acknowledgments

The authors wish to thank L. Silvestroni for preparation of the bulk material and S. Guicciardi for useful discussion on the kinetic curves.

References

1. Opeka, M. M., Talmy, I. G., Wuchina, E. J., Zaykoski, J. A. and Causey, S. J., Mechanical, thermal, and oxidation properties of refractory hafnium and zirconium compounds. *J. Eur. Ceram. Soc.*, 1999, **19**, 2405–2414.
2. Fahrenholtz, W. G., Hilmas, G. E., Talmy, I. G. and Zaykoski, J. A., Refractory diborides of zirconium and hafnium. *J. Am. Ceram. Soc.*, 2007, **90**, 1347–1364.
3. Wuchina, E., Opeka, M., Causey, S., Buesking, K., Spain, J., Cull, A. *et al.*, Designing for ultrahigh-temperature applications: the mechanical and thermal properties of HfB_2, HfC_x, HfN_x and αHf(N). *J. Mater. Sci.*, 2004, **39**, 5939–5949.
4. Opeka, M. M., Talmy, I. G. and Zaykoski, J. A., Oxidation-based materials selection for 2000 °C + hypersonic aerosurfaces: theoretical considerations and historical experience. *J. Mater. Sci.*, 2004, **39**, 5925–5937.
5. Gasch, M., Ellerby, D., Irby, E., Beckman, S., Gusman, M. and Johnson, S., Processing, properties and arc jet oxidation of hafnium diboride/silicon carbide ultra high temperature ceramics. *J. Mater. Sci.*, 2004, **39**, 5925–5937.
6. Bellosi, A., Monteverde, F. D. and Sciti, D., Fast densification of ultra-high-temperature ceramics by spark plasma sintering. *Int. J. Appl. Ceram. Technol.*, 2006, **3**, 32–40.
7. Monteverde, F., Ultra-high temperature HfB_2–SiC ceramics consolidated by hot-pressing and spark plasma sintering. *J. Alloy Compd.*, 2007, **428**, 197–205.
8. Monteverde, F. and Bellosi, A., The resistance to oxidation of an HfB_2-SiC composite. *J. Eur. Ceram. Soc.*, 2005, **25**, 1025–1031.
9. Monteverde, F., Hot pressing of hafnium diboride aided by different sinter additives. *J. Mater. Sci.*, 2008, **43**, 1002–1007.
10. Sciti, D., Silvestroni, L. and Bellosi, A., Fabrication and properties of HfB_2–$MoSi_2$ composites produced by hot pressing and spark plasma sintering. *J. Mater. Res.*, 2006, **21**, 1460–1466.
11. Silvestroni, L. and Sciti, D., Effects of $MoSi_2$ additions on the properties of Hf– and Zr–B_2 composites produced by pressureless sintering. *Scripta Mater.*, 2007, **57**, 165–168.
12. Savino, R., De Stefano Fumo, M., Silvestroni, L. and Sciti, D., Arc-jet testing on HfB_2 and HfC-based ultra-high temperature ceramic materials. *J. Euro. Cer. Soc.*, 2008, **28**, 1899–1907.
13. Berkowitz-Mattuck, J. B., High-temperature oxidation, III zirconium and hafnium diborides. *J. Electrochem. Soc.*, 1966, **113**, 908–914.
14. Parthasarathy, T. A., Rapp, R. A., Opeka, M. and Kerans, R. J., A model for the oxidation of ZrB_2, HfB_2 and TiB_2. *Acta Mater.*, 2007, **55**, 5999–6010.
15. Klein, R., Desmaison-Brut, M., Desmaison, J., Mazerolles, L. and Trichet, M. F. In *High Temperature Corrosion and Protection of Materials 6*, Parts 1 and 2, Proceedings 2004, vol. 461–464, pp. 849–856.
16. Jeng, Y. L. and Lavernia, E. J., Review: processing of molybdenum disilicide. *J. Mater. Sci.*, 1994, **29**, 2557–2571.
17. Natesan, K. and Deevi, S. C., Oxidation behaviour of molybdenum silicides and their composites. *Intermetallics*, 2000, **8**, 1147–1158.
18. Sciti, D., Brach, M. and Bellosi, A., Oxidation behaviour of a pressureless sintered ZrB_2–$MoSi_2$ ceramic composite. *J. Mater. Res.*, 2005, **20**(4), 922–930.
19. Nickel, K. G., Multiple law modeling for the oxidation of advanced ceramics and a model-independent figure of merit. In *Corrosion of Advanced Ceramics*, ed. K. G. Nickel. Kluwer Academic Publishers, Norwell, MA, 1994, p. 59.
20. Veytizou, C., Quinson, J. F., Valfort, O. and Thomas, G., Zircon formation from amorphous silica and tetragonal zirconia: kinetic study and modelling. *Solid State Ionics*, 2001, **139**, 315.
21. Ogbuji, L. and Singh, M., High temperature oxidation behaviour of reaction-formed silicon carbide ceramics. *J. Mater. Res.*, 1995, **10**(12), 3232–3240.